ORIGINAL ARTICLE

Petrophysical characterization of the South Georgia Rift Basin for supercritical CO_2 storage: a preliminary assessment

Olusoga Martins Akintunde ·
Camelia Knapp · James Knapp

Abstract The Triassic–Jurassic South Georgia Rift (SGR) Basin, buried beneath Coastal Plain sediments of southern South Carolina, southeastern Georgia, western Florida, and southern Alabama, consists of an assemblage of continental rift deposits (popularly called red beds), and mafic igneous rocks (basalt flows and diabase sills). The red beds are capped by basalts and/or diabase sills, and constitute the target for supercritical CO_2 storage as part of a Department of Energy funded project to study the feasibility for safe and permanent sequestration. The purpose of this research is to evaluate subsurface suitability for underground CO_2 storage in terms of the local and regional distribution of porous and permeable reservoirs. In addition, unlike shale-capped CO_2 reservoirs, very little is known about the ability of basalts and diabase sills to act as viable seals for CO_2 storage. New results demonstrate the presence of confined porous rocks that may be capable of storing significant quantities of supercritical CO_2. Reservoir thicknesses as high as 420 m and an average porosity as high as 14 % were obtained. The SGR Basin manifests distinct porosity–permeability regimes that are influenced by the depositional environments. These are: a high-porosity, medium/low-permeability zone associated with lacustrine deposits, a medium/low-porosity, low-permeability zone dominated by fluvial fine- to very fine-grained sandstone, and an extremely low porosity and permeability zone characterized by fluvial and alluvial-fan deposits. Analyses further show that the basalt flows and diabase sills are characterized by low porosity as well as high seismic velocities and densities that are favorable to caprock integrity.

**Keywords** CO_2 storage · Porosity · Permeability · Red beds · Diabase sills

O. M. Akintunde (✉) · C. Knapp · J. Knapp
Department of Earth and Ocean Sciences,
University of South Carolina, 701 Sumter Street,
EWS 617, Columbia, SC 29208, USA
e-mail: oakintunde@geol.sc.edu

Introduction and motivation

The interest to curtail rising concentrations of atmospheric CO_2 provides a motivation for geologic CO_2 sequestration. Prior to the industrial revolution (around 1750–1850), global average atmospheric CO_2 were varying slightly between 180 and 280 parts per million by volume (PPMV, Tans 2012). But since the industrial revolution, atmospheric concentrations of CO_2 have increased significantly to present levels of between 390 and 395 PPMV (Tans 2012). This increase has caused a doubling of the global mean surface temperature from 0.4 to 0.8 °C with tendency to significantly impact global climate change in weather patterns (Schaef et al. 2009). The rise in atmospheric CO_2 levels has been attributed to continued increase in global

Fig. 1 Map (modified from McBride et al. 1989) of the areal extent of the South Georgia Rift Basin showing locations of the study
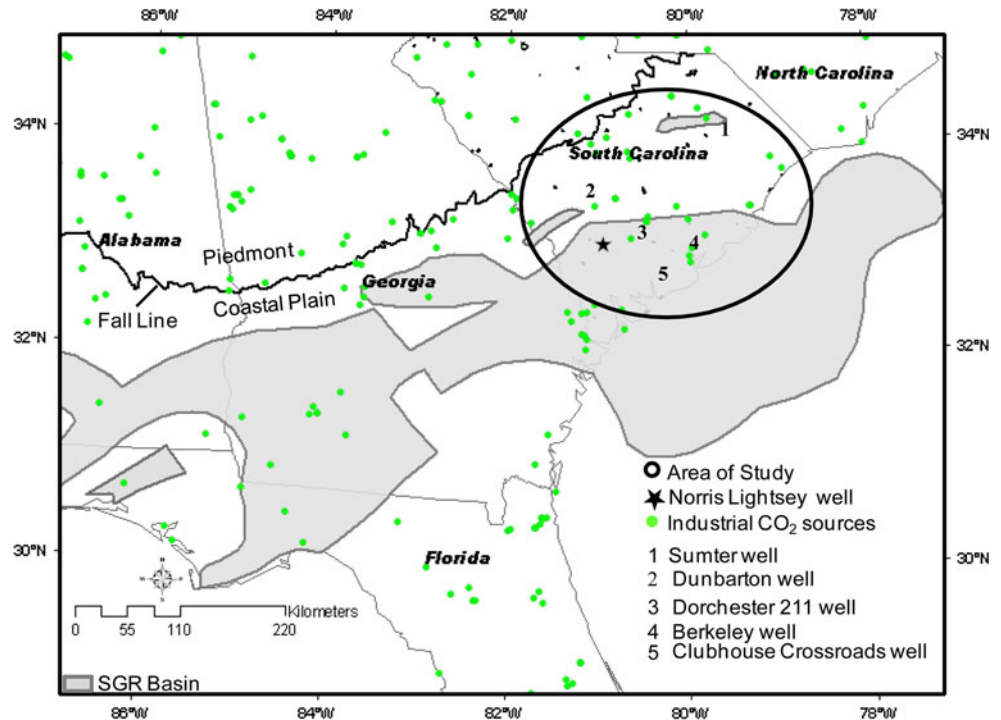
energy use through expanded consumption of fossil fuels (EIA 2007). The twentieth century particularly experienced a tremendous increase in energy consumption. This was caused by expanding human populations worldwide and development of new technologies that rely heavily on combustion of hydrocarbon fuels. The intergovernmental panel on climate change projects that average global atmospheric CO_2 concentration will reach about 750 PPMV by 2100 (EIA 2007). Consequently, the challenge of this twenty-first century is to stabilize atmospheric CO_2 concentrations at 550 PPMV, which are approximately twice preindustrial concentrations (Albritton and Meira Filho 2001). To achieve this based on estimates provided by Albritton and Meira Filho (2001), global emissions must be continuously reduced so that by 2050, global emissions are 15 $GtCO_2$/year (15 billion tons of CO_2 per year) and by 2100, emissions would be 50 $GtCO_2$/year less (1 $GtCO_2$ = 10^9 metric tons of CO_2 = 10^{12} kg of CO_2). To meet the global expectations of reducing CO_2 emissions from sources (such as power generation, iron and steel production, coal mine, heavy manufacturing, and hydrocarbon generation), geologic sequestration is considered one of the preferred choices for near-term mitigation.

Geologic sequestration involves capture, separation, transport and injection of CO_2 into geologic repositories such as deep and unminable coal seams, deep saline aquifers, and mature oil and gas fields. According to Lumley et al. (2010), 4 billion tons (Gt) of CO_2 must be stored for geo-sequestration to make any impact on reducing global CO_2 emissions. Current projections based on active geo-

sequestration projects around the world indicate the need for a dramatic increase in commercial CO_2 projects by a factor of 1,000 or more to achieve the 4 Gt/year (Lumley et al. 2010). It is as a result of this that the push to select and characterize potential sites for CO_2 storage appears to be gaining considerable attention. Of the three geologic sequestration options for carbon capture and storage (CCS), storage in deep saline aquifers has been projected to hold the most combined promise in terms of storage capacity, proximity to emission sources, and state-of-the-art technology (Bachu et al. 1994; Hovorka et al. 2006; Lucier et al. 2006). Deep saline aquifers have very minimal socio-economic benefit for domestic purpose as drinking water and for agricultural usage due to depth of occurrence and high concentrations of dissolved solids.

The presence of these deep saline aquifers capped by Jurassic-age basalt and diabase sills are key factors for CO_2 sequestration within the South Georgia Rift (SGR) Basin. Proximity of these target rocks to known CO_2 sources further underscores prospects for geologic storage (Fig. 1). Furthermore, these saline formations occur well below underground sources of drinking water and at a depth greater than 800 m below the surface to maintain supercritical CO_2 injection. The project goal is to determine subsurface suitability for underground CO_2 storage in terms of: (1) the local and regional distribution of porous and permeable target reservoirs and (2) the viability of the target seals.

The focus of study is on southern South Carolina (Fig. 2) where geologic evidence abounds for potential Triassic–Jurassic formations (Gohn et al. 1983; Gohn
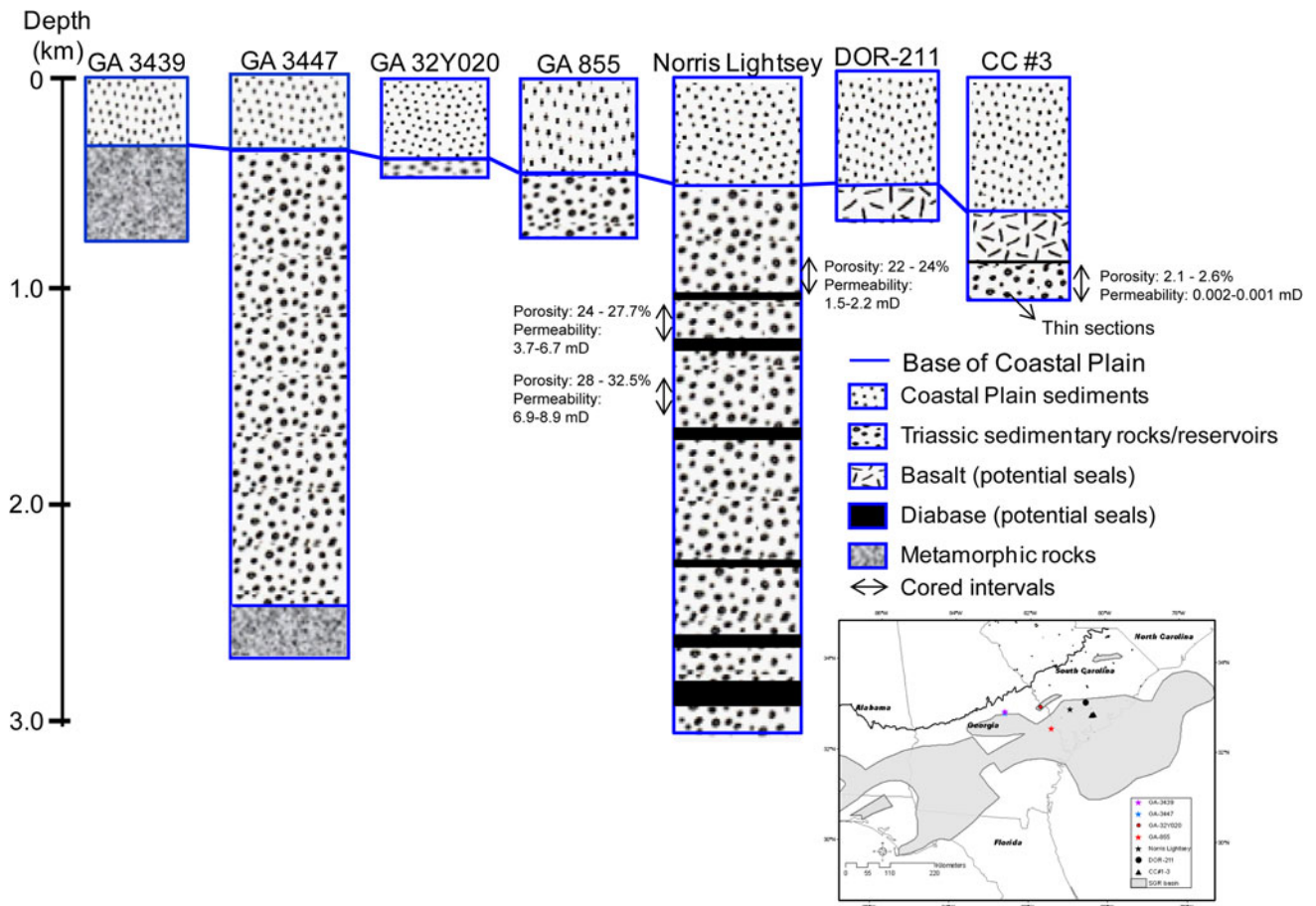
Fig. 2 A generalized stratigraphic column for the SGR Basin (modified from Akintunde et al. 2013). *Inset* is the map of the study locations. Notice the change in subsurface geology from the GA to the SC parts of the basin due primarily to the strong presence of diabase sills and basalt flows

Table 1 A summary of critical rock properties/characteristics required for CO_2 storage

S/N	CO_2 storage requirements	Critical rock properties/characteristics
1	A reservoir with adequate storage capacity	Porosity, permeability, reservoir thickness
2	Reservoir injectivity and/or unrestricted fluid flow	Permeability, porosity, thickness
3	Trapping mechanism to ensure containment of CO_2	An overlying caprock or seal
4	Seal integrity and viability	Porosity, permeability, thickness
5	Knowledge of the physics of CO_2–rock interactions for the purpose of fluid monitoring	Porosity

1983; Smyth 2007; Goldberg et al. 2010) that are worth evaluating for storage capacity, reservoir quality and injectivity as well as seal viability for the purpose of sub-surface CO_2 storage (Table 1). According to the Carbon Sequestration Atlas of the United States and Canada, there is a high concentration of carbon sources located over the SGR Basin. The proximity of carbon sources to promising CO_2 geologic storage formations adds to the relevance of this investigation. If the Triassic/Jurassic saline formations within the SGR Basin prove to be a suitable carbon storage option, then the co-location with substantial carbon sources makes carbon sequestration very attractive. Of critical importance to these characteristics (Table 1) are the need to understand the local and regional distribution of porosity and permeability, and how these reservoir properties may be impacted by depositional environments. Results of analysis of experimental data and petrophysical interpretation of well logs carried out to evaluate these properties and their potential implications for supercritical CO_2 storage are presented.

Why supercritical CO_2 storage?

At depth below 800 m, CO_2 injected into the subsurface under normal geothermal conditions with near hydrostatic

pressures will exist in supercritical state (Burruss et al. 2009). In this state, CO_2 has gas-like compressibility, viscosity, and surface tension with liquid-like densities. The consequences are that CO_2 can flow more easily within the confined reservoir and more storage per unit volume can be achieved. In addition, supercritical CO_2 is miscible and soluble in water (Koide et al. 1993). The CO_2, due to its buoyancy, will typically move updip in geologic formations, and tend to accumulate in traps enclosed by a seal. On a short-term, the stored CO_2 can be trapped by structural or stratigraphic seals as observed in hydrocarbon accumulations. Also, the dissolved and immiscible CO_2 can travel within the formation over long residence times in the form of hydrodynamic trapping (Bachu et al. 1994). The long-term trapping usually takes the form of solubility and/or mineral trapping (Koide et al. 1993).

Geologic setting

The SGR Basin is the largest of the Eastern North American Margin (ENAM) rift basins with an area of about 100,000 km^2 and basin fill thickness of 3,500 m (Chowns and Williams 1983). The basin formed in an extensional tectonic setting associated with the breakup of Pangaea and the subsequent opening of the North Atlantic Ocean. The breakup of Pangea started in late Triassic (about 215–175 million years ago), producing a zone of rifting from North Africa to the Gulf of Mexico and along the east coast of North America. Block-faulted basins were produced by this rifting though considerable changes in the relative positions of the continents took place in late Jurassic. Also due to the proximity of the southeastern part of North America to the triple junction between the North Atlantic, South Atlantic, and the Gulf of Mexico, this area was susceptible to complex rifting and transform faulting (Chowns and Williams 1983; McBride et al. 1989). The SGR Basin is also known to have a complex and irregular horst and graben systems (Daniels et al. 1983). Reflection seismic studies by McBride et al. (1989) characterized the basin to be a composite of individual syn-rift, half-grabens separated by intervening structural highs. Studies by Petersen et al. (1984), Heffner et al. (2012) and Akintunde et al. (2013) have also shown the SGR Basin to be a composite of smaller Triassic basins which include the Dunbarton basin in South Carolina (Marine and Siple 1974).

Stratigraphically (Fig. 2), the basin is filled with sedimentary rocks including sandstones, mudstones, siltstones and conglomerates, as well as mafic igneous rocks such as basalt flows and diabase sills. The basalt flows and diabase sills were emplaced between about 200 and 170 million years ago (Hames et al. 2000) as a result of igneous activity associated with the formation of the basin. These Triassic–Jurassic

rocks are buried entirely below the Cretaceous–Cenozoic Coastal Plain sediments in South Carolina, Georgia and parts of Alabama and Florida, and are separated from the Piedmont province by the Fall Line (Fig. 1).

Objectives and methods

This research is designed to investigate subsurface suitability for CO_2 storage in terms of the local and regional understanding of rock properties such as porosity and permeability that are critical for CO_2 storage (Table 1). The study is also concerned with the need to determine the physical properties including internal composition and microstructure of the seals as well as to understand the impacts of depositional and/or post depositional processes on rock properties. Laboratory experiments involving standard measurements of in situ porosity, permeability, density and ultrasonic P-wave velocity (Prasad 2002; Schon 2011) were carried out on borehole samples from Sumter, Berkeley, Dorchester-211 and Clubhouse Crossroads wells (Fig. 1). Existing core laboratory data from Dunbarton (Marine and Siple 1974; Marine 1974) and Norris Lightsey well (Fig. 1) were used to supplement the new porosity and permeability data. Identification and characterization of seals and reservoirs were based on the recognition criteria for lithology from well logs presented in Table 2 as well as detailed analyses of cores, thin sections (Gohn et al. 1983), X-ray diffraction (XRD) data (Table 3) and X-ray computed tomographic (CT) images (Ketcham and Carlson 2001). Steps employed to analyze

Table 2 Recognition criteria for lithology from borehole logs with penetrations of the SGR Basin-fill

S/N	Well logs' response	Interpretation
1	High resistivity (<200 Ωm) from deep induction electrical log (ILD) coupled with low gamma ray (<10 API) and high velocity[a] (>5.5 km/s)	Indicative of a low porosity and impermeable diabase sill and/or basalt
2	Low resistivity (5–10 Ωm) from deep induction electrical log (ILD) coupled with high gamma ray (50–100 API) and velocity[a] (4–5 km/s)	Indicative of fine-grained Triassic sedimentary rocks (commonly sandstone interbedded with mudstones and siltstones)
3	Medium resistivity (up to 70 Ωm) from deep induction electrical log (ILD) coupled with high gamma ray (up to 100 API)	Indicative of unconsolidated Cretaceous Coastal Plain sediments (typically filled with fresh water)

Interpretation of log response aided by available lithology data from the Norris Lightsey and Georgia 855 wells (Fig. 2)

[a] Velocity derived from sonic log

Table 3 Sandstone composition from X-ray diffraction analysis on selected samples from Sumter, Berkeley and Clubhouse Crossroads-3 wells (CC-3-1 and CC-3-2)

Mineral name	Sumter (%)	Berkeley (%)	CC-3-1 (%)	CC-3-2 (%)
Quartz	35	19	18	19
K-feldspar	21	8	6	22
Plagioclase feldspar	–	12	<5	13
Mica/illite	5	24	29	5
Smectite	22	15	15	14
Chlorite	–	–	10	5
Kaolinite	10	10	–	–
Calcite	–	–	12	19
Hematite	–	<5	5	<5

Sumter (conglomerate at 213.6 m), Berkeley (fine-grained sandstone at 548.34 m), CC-3-1 (fine-grained sandstone at 1,047 m), and CC-3-2 (coarse-grained sandstone at 1,146 m)

porosity and permeability data (Table 4) and estimate the storage capacity are presented in "Porosity and permeability of sandstones/red beds" and "Estimation of CO_2 storage capacity".

The basalt flow deposits

The Clubhouse Crossroads (CC-1, CC-2 and CC-3) and the Dorchester-211 (DOR-211) wells in southern South Carolina (Fig. 1) are two examples of known occurrence of Jurassic age basalt flows (Lanphere 1983, Hames et al. 2000) within the SGR Basin that could serve as viable

CO_2-reservoir seals. The CC-1, CC-2, and CC-3 wells covered total depths of 792, 907, and 1,152 m and penetrated 42, 131, and 256 m thicknesses, respectively, of basalt (Gohn et al. 1983). DOR-211 covered a total depth of 632 m and penetrated a 32-m thick of basalt deposit (Reid et al. 1986). These basalt flows have been studied for geologically, tectonic and regional significance (Chowns and Williams 1983; McBride et al. 1989; Akintunde et al. 2011; Heffner et al. 2012). However, a knowledge of the physical properties of these rocks is necessary to assess seal's viability is lacking. Shown in Figs. 3 and 4 are X-ray CT scans of cores from these wells. The highly vesicular flow top (Fig. 3) is characterized by spheroidal pores and appears to have undergone significant alteration. The alteration may result from weathering, erosion, magmatic and other tectonic processes based on petrographic and geochemical evidence (Gottfried et al. 1983). The interior of flow typically retains the dark color and the fine-to-median grained characteristics (Figs. 3, 4). The vesicles within the flow top are represented by the black spheroidal pores in the CT image. The presence of olivine and pyroxene are represented in white. The significant difference in the gray shades between the flow top and the flow interior is due to variations in the mineralogical composition as well as the proportion of pore space. The interior of the flow consists of minerals such as plagioclase, pyroxene and olivine (Gottfried et al. 1983). In addition, these do not have pores and are dominated by minerals resulting in the whitish, gray color. Additional insights into the texture and internal composition of the basalt flow interior are provided in the

Table 4 Porosity and permeability measurements

S/N	Sample ID	Depth (m)	Porosity (%)	Permeability (mD)	Source (year)
1	Sumter	213.06	10.6	0.16	This study: WL (2011)
2	Berkeley_1	548.34	13.3	0.15	This study: WL (2011)
3	Berkeley_1[a]	548.34	13.0	0.10	This study: CSM (2011)
4	Berkeley_2	556.56	8.6	0.01	This study: WL (2011)
5	Berkeley_2[a]	556.56	8.9	0.01	This study: CSM (2011)
6	Dunbarton	821.13	6.3	0.016	Marine and Siple (1974), Marine (1974)
7	Norris Lightsey_1	987.86	22.6	1.5	CL (1984)
8	Norris Lightsey_2	988.47	23.8	2.2	CL (1984)
9	Norris Lightsey_3	1,040	24.2	6.7	CL (1984)
10	Norris Lightsey_4	1,059.2	27.7	3.7	CL (1984)
11	Norris Lightsey_5	1,505	28.1	8.9	CL (1984)
12	NorrisLitghtsey_6	1,522	32.5	6.9	CL (1984)
13	Clubhouse Crossroads-3_1	1,047	2.6	0.001	This study: WL (2012)
14	Clubhouse Crossroads-3_2	1,146	2.1	0.0023	This study: WL (2012)

[a] Measurements of the Berkeley samples were repeated at the Weatherford and CSM laboratories. Core-derived porosity measurements for the Norris Lightsey fall within the range of log-derived porosity values (Table 3). Data sources: WL, Weatherford Laboratories, Golden, Colorado, USA; CSM, Rock Abuse Laboratory, Colorado School of Mines; CL, Core Laboratory Petroleum Engineering, Dallas, Texas. Apart from Sumter and Clubhouse Crossroad-3_2 that are coarse grained/conglomeratic sandstone, other locations are fine-grained sandstone

Fig. 3 X-ray computed tomographic (CT) images of basalt flows encountered at the Clubhouse Crossroad Well #2. The highly vesicular top of flow at 726 m and an interior layer at 802 m are illustrated on the left and right. The CC-2 flow interior at 802 m appear fresh, un-weathered and show physical characteristics similar to the DOR-211 sample (Fig. 4)
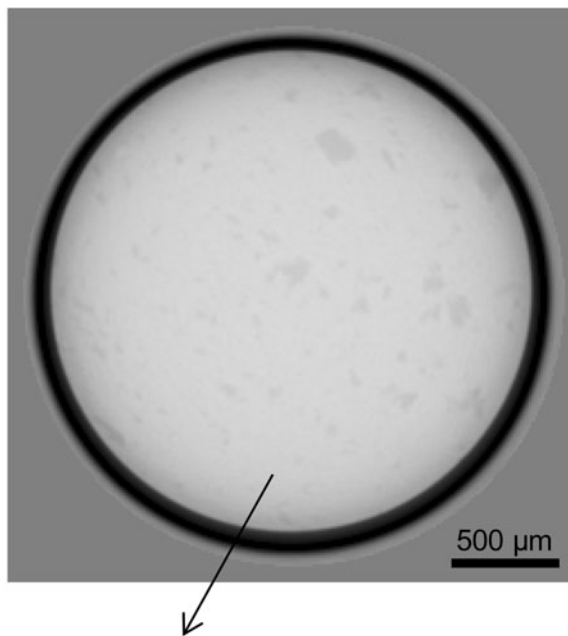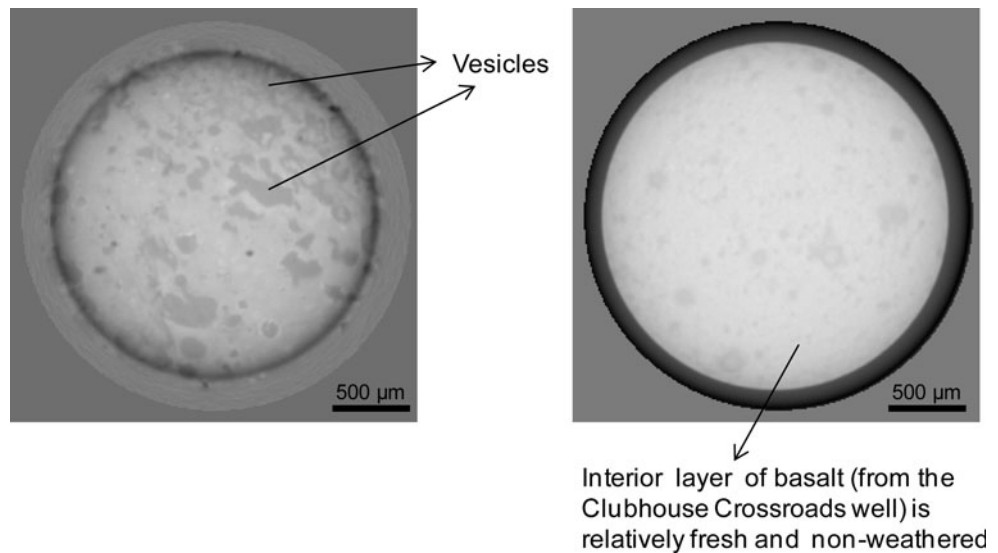
Fig. 4 X-ray computed tomographic image of an interior basalt layer encountered at Dorchester-211 well at 605 m

Fig. 5 A photomicrograph of Dorchester-211 basalt flow at 600 m in plain white light. *The yellowish clasts* represent olivine-normative/altered basalt

thin section/photomicrograph shown in Fig. 5 for the DOR-211 sample. The fine-grained, porphyritic and crystalline nature of the sample can be seen coupled with the presence of yellowish olivine, black augite, and gray stratiated plagioclase phenocrysts in a ground mass of whitish feldspar. Slight textural and mineralogical alteration, common in basalt, can be seen in the yellowish clasts (olivine-normative/altered basalt) as well. This is
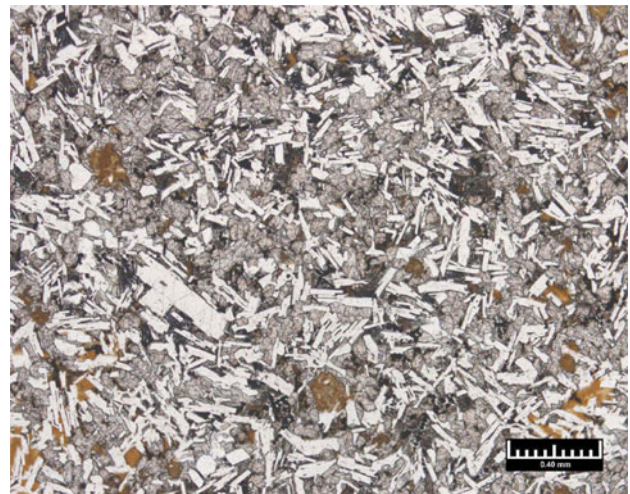
possibly caused by magmatic processes or local/regional scale metamorphism associated with extensional tectonic movements of the SGR Basin.

The basalt flow layers above the top of flow are generally denser, fresher and characterized by higher seismic velocities than the flow top. The densities measured were 2.72 and 2.89 g/cm^3 for the CC-2 and DOR-211 flow interiors and 2.28 g/cm^3 for the CC-2 flow top (Figs. 4, 5). Ultrasonic measurements yielded P-wave velocities (V_p) of 3.70 km/s for the CC-2 flow top as well as 6.20 and 6.75 km/s for the CC-2 and DOR-211 flow interiors at 802 and 605 m. With the exception of the flow top that produces porosity of 14.34 % and permeability of 0.045 mD, near-zero porosity and permeability values were obtained for the interior layers.

Diabase/palisade sills

An extensive suite of diabase sills that could serve as caprocks for CO_2 storage exists within the SGR Basin (Fig. 6). The diabase sills are easily identified from the recognition criteria shown in Table 2. These diabase sills occur well below the 0.8- to 1-km depth required for supercritical CO_2 storage and range in thicknesses from 1.5 to 124 m as shown in the Norris Lightsey well (Fig. 2). This well was a wildcat drilled to a depth of about 4,000 m

in northwest Colleton County, SC. It encountered over 3,100 m of Triassic red beds confined above and below by diabase sills. The principal minerals are plagioclase, pyroxene and olivine though interstitial growths of accessories such as biotite, quartz and potassium feldspar can be seen (Fig. 7). Most of the diabase encountered in the SGR basin is phaneritic because of the diabasic (intergranular) to ophitic texture depending on grain size. The observed change in gray shades in the CT images (Fig. 7) is due to the differences in the mineralogical composition and/or

Fig. 6 A section from the Norris Lightsey well log in Colleton County, South Carolina (Fig. 1) shows target red bed reservoir overlain by diabase sill. The diabase sill is easily delineated from the underlying and overlying clastic reservoir units by its low gamma ray, high resistivity and high velocity
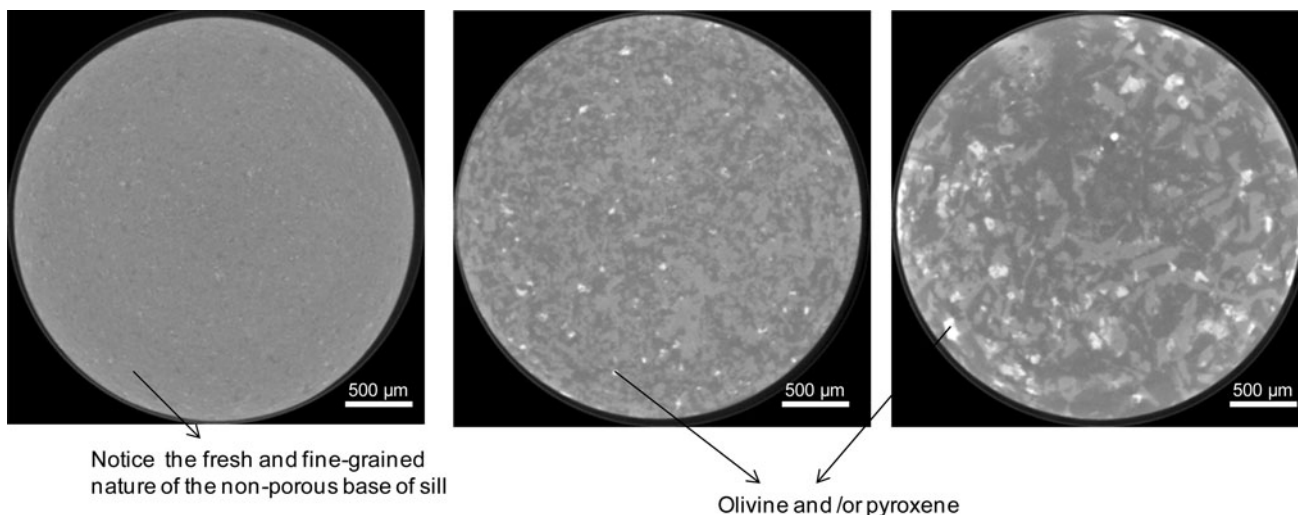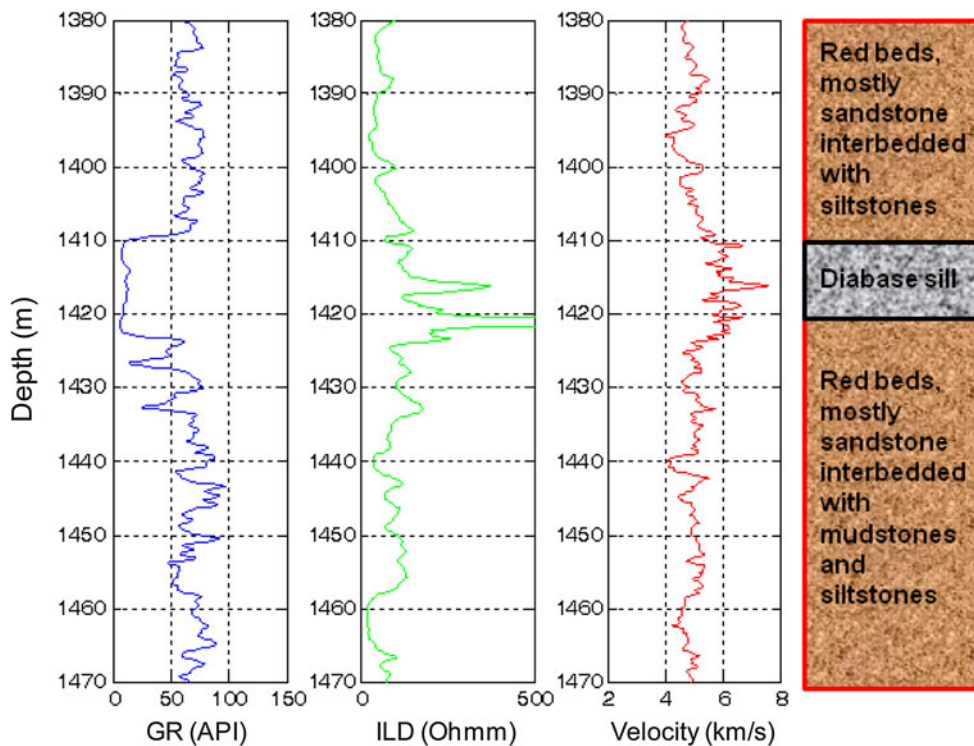

Fig. 7 X-ray computed tomography (CT) scans/images obtained for samples of diabase/palisade. From the *left to right* are samples within 2, 20 and 200 m respectively of the base of sill. *Changes in gray* levels are indicative of variations in the density of minerals

texture of the tested samples. The whitish marks represent olivine and pyroxene, and mineralogical alterations caused by possible crystallization processes are common within the diabase. Olivine is particularly susceptible to alteration and in thin sections has been shown to correspond to pseudomorphs of serpentine, idingsite, and magnetite (Chowns and Williams 1983). Relatively uniform P-wave velocities (5.20–5.50 km/s), and densities (2.98–3.00 g/cc), respectively, were observed for the diabase/palisade sills. Because these are much shallower samples occurring within 250 m from land surface, the velocities are lower than the sonic-derived velocities from the log (Fig. 6) that shows values exceeding 6 km/s.

Basalt flows versus diabase sills

For the purpose of subsurface characterization and to assess their effectiveness as CO_2 reservoir seals, it is important to make a distinction between basalt flows and diabase sills. Based on the core-scale laboratory measurements, the interior of the SGR basalt flow could serve as a seal because it is dense, impermeable and non-porous. In addition, the overlying, highly vesicular and porous top of flow has the ability to contain and mineralize the CO_2 that may tend to migrate upward or escape from the interior layer (Schaef et al. 2009; Goldberg et al. 2010). The ability of the highly vesicular basalt flow tops to rapidly absorb and chemically react with CO_2-saturated pore water forming stable carbonate minerals makes basalt formation a potential geologic storage option for CO_2 (McGrail et al. 2006; Schaef et al. 2009; Goldberg et al. 2010). However, the non-homogeneous nature of the basalt flow (McGrail

et al. 2006; Planke et al. 1999) coupled with its restrictive occurrence within the SGR Basin (Akintunde et al. 2011; Heffner et al. 2012; Akintunde et al. 2013) could be an issue for the regional scale subsurface potential for CO_2 storage. In this situation, more drilling would be needed to support seismic evidence for delineation of true geographical extent of the basalt flows. In addition, the rate of basalt mineralization can be different for different geologic environments. Hence, an understanding of the SGR-basalt CO_2-brine interactions as a function of temperature, pressure and rock composition would be necessary. In contrast, the diabase sills appear to exhibit very little variations in measured velocities and densities. Also within the SGR Basin and unlike the basalt flows, evidence from deep borehole abounds for the occurrence of these sills at depths that favor supercritical CO_2 storage.

Red beds reservoir

The late Triassic–Early Jurassic red bed units are overlain by and/or interbedded with basalt flows as seen in the Clubhouse Crossroad well-3 (Gottfried et al. 1983). Intrusion of these red beds by diabase sills is evident from the Norris Lightsey well (Fig. 2). Apart from the Norris Lightsey well, the CC-3 well remains the only other well with deep penetrations of the red beds. Located in southwestern Dorchester County near Charleston South Carolina (Figs. 1, 2), CC-3 was drilled alongside CC-1 and CC-2 by the US Geological Survey between 1975 and 1977. It penetrates 121 m of red beds between 1,031 and 1,152 m. This formation is overlain by 256 m of basalt flows, and 775 m of Cretaceous and Cenozoic sediments of the

Fig. 8 Triassic red bed cores (1.5-in. diameter) recovered from the CC-3 well. *Left* is fine-grained sandstone sample at depth of 1,047 m while the core on the *right* is coarse-grained/conglomeratic sample at depth of 1,146 m. *The grayish green* seen on the fine-grained sample are small pockets of siltstone and granite clasts and the ones on the coarse-grained are predominantly granitic clasts

Granitic clasts in both fine-grained (left) and coarse grained (right) red beds
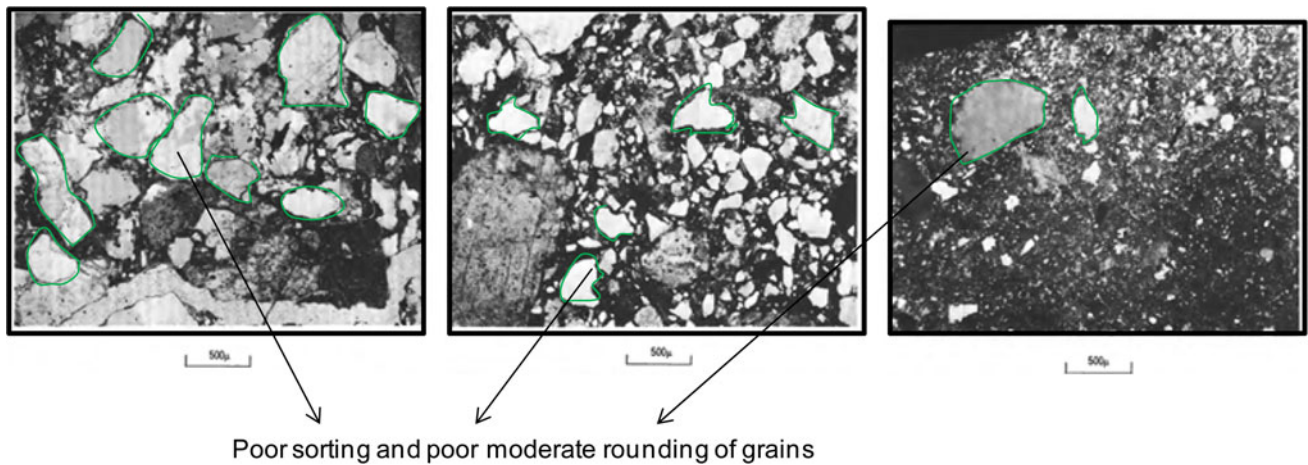
Poor sorting and poor moderate rounding of grains

Fig. 9 Photomicrographs (modified from Gohn et al. 1983) of thin sections of coarse grained sandstones within close proximity of the coarse grained sample at 1,146 m that we used in this study (Fig. 8 above). From *left to right* are sandstone at 1,146.9 m (in plane light), 1,146.6 m (in plain light) and 1,146.7 m (in crossed nicols). Poor sorting and poor moderate rounding of grains (*green marks*) can be seen in all three sections

Coastal Plain. There are no geophysical borehole logs for the CC-3 red bed section. Interpretation of cores, well and XRD data (Table 2) together with analysis of existing geologic records from Gohn et al. (1983), Marine and Siple (1974) and Marine (1974) enable the identification of two dominant facies of red beds representative for the SGR Triassic-basin fill. These are fine-to-medium grained and coarse-grained sandstones or conglomeratic sandstones (Fig. 8). The fine-to-medium grained facies are poorly sorted and well consolidated. These are primarily reddish sandstones commonly interbedded with mudstones and siltstones. Thin layers of conglomerate and shale are also present.

The dominant minerals based on the XRD analysis of selected samples from Berkley, Sumter and Clubhouse Crossroads-3 (CC-3-1) include quartz, feldspar, smectite and illite/mica (Table 3). The coarse-grained facies are well-indurated based on the core examination. These are mostly characterized by poorly sorted coarse-grained to conglomeratic sandstones and interbedded mudstones. The mudstones are similar to the ones encountered within the fine-to-medium grained facies. An excellent example of these facies is found directly below the fine-grained sample in the CC-3 well (Fig. 8). The significant color change in the coarse-grained sample is due to the presence of granitic and other detrital clasts such as granodiorite, mylonite, microbreccia and basalt. The dominant minerals in the coarse-grained sample are quartz and feldspar based on XRD analysis and thin sections (Fig. 9). The XRD data (Table 3) indicates lack of textural and compositional maturity for both the fine-grained and coarse-grained samples due to their high proportions of unstable grains and/or lithic fragments. This substantiates the petrological evidence for the lack of maturity of these red beds reported in Gohn et al. (1983).

The poorly sorted character of both fine- and coarse-grained sediments could have a significant impact on the permeability of these formations. Poorly sorted and fine-grained sandstone usually has smaller pore throats with a consequent reduction in permeability. Photomicrographs of thin sections (Fig. 9) provide evidence for poor sorting and moderate-to-poor rounding of grains within the coarse-grained sediment.

Porosity and permeability of sandstones/red beds

Experimentally derived porosity and permeability values on samples from Berkeley, Sumter, Dunbarton, Norris Lightsey and Clubhouse Crossroads-3 wells (Fig. 1) identify four distinct porosity–permeability regimes within the SGR Basin (Table 4; Fig. 10). These are: (a) a high-porosity, medium/low-permeability zone associated with the Norris Lightsey well's lacustrine deposits, (b) a medium/low-porosity, low-permeability zone observed in the Berkeley and Sumter fluvial sandstones, (c) a low-porosity, low-permeability zone associated with Dunbarton and Berkeley fluvial deposits, and (d) an extremely low porosity and permeability associated with fluvial–alluvial deposits found in the Clubhouse Crossroads (CC-3) red beds. The lacustrine origin for the high-porosity medium/low-permeability zone derives from the recovery of pollen and spore assemblages from drill cuttings of gray-green shales between 1,373 and 2,184 m depth in the Norris Lightsey well (Traverse 1987). These deposits according to Traverse (1987) resemble lacustrine sequences in other exposed basins (Olsen et al. 1991). Evidence for lacustrine deposition from this study comes from the analysis of the Norris Lightsey well logs (Fig. 6). The presence of lacustrine deposits within the SGR Basin is also supported by

Fig. 10 Permeability–porosity plot based on experimental data from study locations
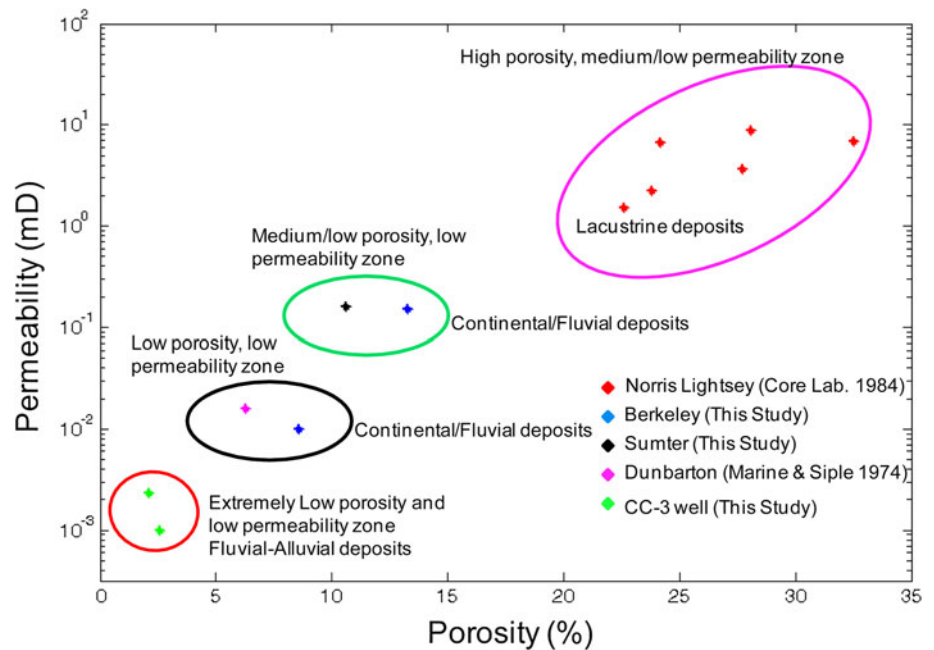
Ziegler (1983) who identified a prominent belt of seismic reflections near the middle of the Triassic sequence in the South Georgia basin as lacustrine. Of importance to subsurface evaluation for CO_2 storage are the observed significant variations in the porosity–permeability distribution especially within the high porosity, medium/low permeability associated with the Norris Lightsey's lacustrine fine-grained sandstones. Though there are no thin sections for the Norris Lightsey well, the presence of fine-grained siltstones (Fig. 6) provides indication of poor sorting. The fine-grained siltstones are generally characterized by very limited and/or fewer less interconnected pores with a consequent reduction in permeability.

The variation in the amounts of silt and clay particles as well as the differences in grain sizes could be a plausible explanation for the Norris Lightsey permeability-porosity trends. A high-porosity–low-permeability trend can also be observed within this zone. Given the volumetric relationship between porosity and permeability, it appears logical to expect high porosities to correspond to high permeability within the same formation. However, this is not always the case in this study area. It is possible for a rock sample to have high porosity and low permeability. Unlike porosity that depends primarily on the volume properties of the pores, permeability is a function of both the volumetric and geometric properties of the rock pores (Prasad 2003). Any variation in pore geometry will affect permeability. As pointed out in Mavko et al. (2003), two sandstone samples can exhibit the same porosity and microstructure, but different average grain sizes leading to the larger grain size with a higher permeability. In addition, the relatively high percentage of silt and clay for the Norris Lightsey samples

(Core Laboratories Report 1984) suggests a possible cause of the low permeability. This (according to the Core Lab. Report) may be partially due to a shattering of the matrix material by the impact of the sidewall sampling device.

The interpreted fluvial/continental and fluvial/alluvial origins for the medium/low-porosity, low-permeability zone as well as the low/extremely low porosity and low/extremely low permeability zones are based on lithological similarities with exposed analog basins characterized by deposition in these environments. These exposed Triassic–Jurassic basins are prominent within the Newark Super group and other parts of south eastern United States (Gohn et al. 1983; Olsen et al. 1991). The absence of textural and mineralogical maturity in the sandstones within these zones based on XRD analysis (Table 3) favors deposition by fluvial processes. Another evidence for fluvial deposition from this study derives from a re-analysis of cores of Triassic red beds from Dunbarton (Fig. 1) shown in Marine (1974). The lithologsy and depositional history of the poorly sorted Dunbarton red beds is consistent with the geology of fluvial deposits as shown in Miall (1996). The basis for the interpreted fluvial/fluvial–alluvial depositional environment for the low/very low porosity and permeability for the Triassic red beds recovered from the Clubhouse Crossroad (Fig. 8) and was based on geologic evidence from Gohn et al. (1983) and Lindholm et al. (1979). While the low/very low porosity–permeability of the fluvial–alluvial deposits may appear unique to the SGR Basin, low/very low porosity–permeability is not uncommon in poorly sorted fluvial sandstones (Nelson 2004). The low porosity and permeability markers within these zones are due to the poor sorting and small pore throats exhibited by these sandstones (Figs. 8, 9).

Fig. 11 Gamma ray (GR), deep induction resistivity (ILD), acoustic transit time (*t*) and porosity. Porosity estimated from the sonic log (acoustic transit time) over the depth interval shown using the Wyllie time average formula (Wyllie et al. 1956)
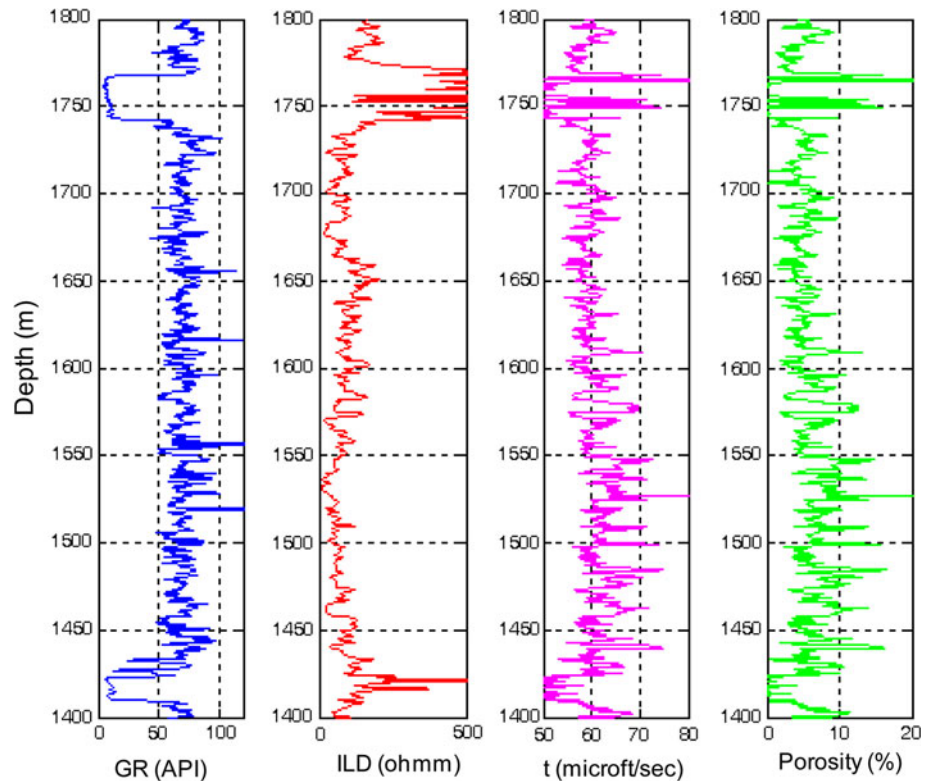
Estimation of CO$_2$ storage capacity

The amount of CO$_2$ that can be stored within the confined porous reservoir (Figs. 2, 11; Table 4) must be taken into consideration to decide whether or not subsurface storage would be a worthwhile effort. Porosity values (Table 1) were derived from red bed intervals in the Norris Lightsey well (Fig. 2). These were calculated over the intervals with reservoir and seal presence (Table 5). A variety of well logs was used to aid accurate interpretations for porosity, and an example is shown in Fig. 11. Porosity (ϕ) was calculated from the sonic log using the Wyllie time average formula:

$$\phi = (\Delta t - \Delta t_{\mathrm{ma}})/(\Delta t_{\mathrm{f}} - \Delta t_{\mathrm{m}}a),$$

where Δt is acoustic transit time, Δt_{ma} is acoustic transit time of the rock matrix and Δt_{f} is acoustic transit time of interstitial fluids (Wyllie et al. 1956). The inputs into this formula are all in µs/ft. Acoustic transit time was obtained from the sonic log and 52.6 and 89 µs/ft were used as the acoustic transit time of the rock matrix and acoustic transit time of interstitial fluid (brine), respectively (Mavko et al. 2003). Because of the significant variations in the log-derived porosity measurements, an average value was used in the storage capacity calculations. It is important to note that the core-derived porosity measurements (Table 4) fall within the range of the log-derived values (Table 5). The differences are due to the difference in scale of measurements.

For storage capacity estimation, a theoretical approach based on the DOE-NETL equation (DOE 2008) was used. It estimates CO$_2$ storage capacity (GCO$_2$) based on the following expression:

$$\mathrm{GCO}_2 = A \times h \times \phi \times \rho \times E,$$

where A is the geographical area covered by target reservoir and seal, h is reservoir thickness, ϕ is reservoir porosity, ρ is density of CO$_2$ and E is storage efficiency factor.

A conservative, projected minimum value of 5,000,000 (m^2) was used for the geographical area, which covers the region penetrated by red beds and diabase within the study locations. Reservoir thickness determined from well logs and a density of 700 kg/m^3 was used for supercritical CO$_2$ (Burruss et al. 2009). The storage efficiency is the ratio of used space for CO$_2$ storage to the available space multiplied by 100 and an estimate of 10 % was used based on petrophysical interpretations from well logs and core measurements. The results show that 3.73–13.23 GtCO$_2$ may be stored within the study area (Table 5).

Discussion

The SGR Basin has never been previously explored for carbon sequestration in terms of key rock properties significant for CO$_2$ storage. This research is concerned with

Table 5 Storage capacity estimation over target intervals (Fig. 6)

Depth interval (m)	Thickness (m)	Area (m²)	Density of CO_2 (kg/m³)	Porosity range (%)	Average porosity (%)	Storage efficiency (0 %)	CO_2 storage capacity (Gt)
1,240–1,390	150	5,000,000	700	5–22	7.1	10	3.73
1,433–1,733	300	5,000,000	700	5–20	7.7	10	8.10
1,780–2,200	420	5,000,000	700	1–10	3.7	10	5.44
2,310–2,580	270	5,000,000	700	1–22	14	10	13.23

evaluating the critically important reservoir/seal properties necessary to study the feasibility for subsurface storage of CO_2 (Table 1). New experimental and petrophysical results indicate that porous, deep and thick saline Triassic red bed formations with potential for supercritical CO_2 storage do exist within the basin. Injectivity tests and reservoir simulation models will be necessary to know how much can be safely and permanently stored under dynamic reservoir conditions (temperature, pressure and time as well as the kinematics of the rock–CO_2/brine interactions). This would be important to design strategies for long-term storage should CO_2 injection be undertaken.

Basalts and/or diabase sills (Figs. 2, 3, 4, 5, 6, 7) in the area of interest have the physical properties and microstructural conditions required for cap rock integrity. Unlike the top of flow characterized by high porosity, near-zero porosity and permeability values were obtained for the interior of basalt flows. These are consistent with sealing requirements and suggest the basalt may provide viable seals to prevent upward migration of CO_2 into the overlying Coastal Plain sediments. The presence of significantly high pores within the flow top is responsible for the relatively high porosity. In addition, the non-porous and impermeable nature of the interior layers is consistent with their characteristic high velocity values. These are extremely tight, dense rocks with no obvious sign of weathering and any significant micro-structural features that could compromise cap rock integrity. The weathered, poorly consolidated nature and low density of the top of flow are responsible for the low V_p.

However, the diabase sills present a more viable option for further characterization within the SGR Basin in view of the restrictive regional extent of the basalt flow (Akintunde et al. 2013). The high velocities of the diabase sills are similar to velocity values seen in impermeable and non-porous rocks with proven seal integrity either for hydrocarbon or CO_2 sequestration. The X-ray CT scans (Fig. 7) do not reveal any internal features that could compromise the caprock integrity. These sills are fresh, hard rocks and with no indication of any void, opening or pathways that could cause fluid movement. The lack of pores and/or interconnectivities within the base of the diabase sills would enhance the ability to retard upward

migration of CO_2 into the overlying layers. In addition, multiple layers of diabase in association with the confined red beds or sandstone units provide an added advantage for increased physical trapping and/or multiple storage units. Additional studies involving seismic imaging, micro-seismic characterization, borehole imaging, and geomechanical tests are necessary to further evaluate the seal integrity and continuity.

On the basis of porosity–permeability analysis (Fig. 10), two end members or regions of porosity–permeability distribution have been recognized within the SGR Basin. The fluvial/fluvial–alluvial dominated sandstones where the porosity and permeability are lower relative to the lacustrine dominated porosity–permeability region. In between these end members, there are significant variations in the porosity–permeability distribution. This has implications for the degree of reservoir quality and injectivity. These variations also suggest the presence of moderately to highly compartmentalized reservoir system within the SGR Basin. In the fluvial region, the poor sorting effectively limits the pores and pore throats within the rock and with a consequent reduction in permeability. In addition, low permeability behavior is a common feature in the lacustrine region. The consequence of the low permeability is a restriction in subsurface fluid movement, which would impact reservoir injectivity. While the lacustrine deposits will be more viable for the SGR Basin CO_2 storage, a restrictive fluid movement will be unfavorable to commercial scale development should CO_2 injection be undertaken.

Besides the influence of depositional setting, effects of post depositional processes such as compaction and diagenesis are the possible causes of the low porosity and permeability. However, the fact that these are deeply buried rocks, which in some areas are overlain by thick sequences of consolidated extrusive basalt flows and/or intrusive diabase sills, suggests preservation of the pores and pore throats. While this may hold, the occurrence within the Triassic red beds of pore-filling igneous clasts as observed in the CC-3 red bed section (Fig. 8) is an indication of possible textural and mineralogical alterations that can reduce porosity and permeability. Considerable erosion during late Triassic to early Jurassic as well as

tectonically induced events (such as faulting, emplacement of mafic igneous deposits, uplift and subsidence) that preceded sedimentation near the Triassic–Jurassic boundary may have triggered alterations and diagenesis within these sediments.

In view of the vastly expansive areal extent of the basin (about 100,000 km^2), it is strategically and economically important, as part of site characterization studies to know which part of the basin to focus future research efforts and resources available for long-term storage feasibility studies. The Norris Lightsey area (Fig. 1) offers the most promising reservoir conditions for subsurface CO_2 storage. In addition to the geo-sequestration significance of the results of this study, this work demonstrates the applicability of petrophysics or rock physics to regional site characterization in environmental-related studies involving evaluating feasibility for CO_2 storage. Rock physics is commonly applied for monitoring and verification studies. By implementing physics-based laboratory experiments on rock samples, key rock attributes that are strategic and extremely important to the goal of site selection and characterization can be determined. The integration of core scale petrophysical data from multiple wells provides the framework or basis to upscale core derived reservoir properties to regional scale. Seismically constrained 3D geo-reservoir modeling incorporating lithofacies and petrophysically derived rock properties can be implemented using recent geo-statistical rock physics techniques (Spikes et al. 2007; Grana and Della Rossa 2010) to upscale to the regional scale. More data from coring, geomechanics and 3D seismic imaging would be needed to further characterize the geometry, regional extent and continuity of the petrophysically identified reservoirs and seals.

Conclusions

Confined, porous Triassic red bed reservoir units with potential for supercritical CO_2 storage exist within the SGR Basin. Between 3.73 and 13.23 Gt of CO_2 may be stored for a single storage system (and up to 30.07 Gt for a stack storage system). A unique characteristic of the basin revealed by this study is the presence of distinct porosity–permeability regimes that are influenced by the depositional environments. These are: (1) a high-porosity, low/medium-permeability zone; (2) a medium/low-porosity, low-permeability zone; (3) a low-porosity, low-permeability zone, and (4) an extremely low porosity and low permeability zone. The high-porosity, low/medium-permeability zone is associated with lacustrine deposits and consists of fine-grained Triassic sandstones with interbedded layers of siltstone and mudstone. The medium/low porosity, low permeability zone is dominated by fluvial

fine- to very fine-grained sandstone, while the extremely low porosity and permeability zone is characterized by fluvial and alluvial-fan deposits. Presence of low-permeability red beds is a common characteristic within the basin. The low permeability is caused by poor sorting and small pore throats. Tectonically induced post-depositional processes are also possible controls on the observed porosity–permeability trends. The basalt flows and diabase sills possess physical properties (such as high seismic velocities and densities), petrophysical characteristics and micro structural properties consistent with sealing requirements. The diabase sills are distinct from the basalt flows by exhibiting very little variations in velocity and density. This work has shown that rock physics or petrophysics can be applied to subsurface characterization involving environmental-related issues like CCS. It is important as part of a regional site investigation to select an optimum location for drilling to understand changes or variations in reservoir properties at desirable resolution (cm/core/log scale) not provided at the seismic scale.

References

Akintunde OM, Knapp C, Heffner DM, Knapp JH, Shafer J (2011) Reinterpretation of the "J" basalt reflector from seismic data reprocessing across the coastal plain of southeastern Georgia: potential implications for long-term CO2 sequestration. AAPG, Annual Convention and Exhibition, Houston, Texas, AAPG Search and Discovery Article #80174

Akintunde OM, Knapp CC, Knapp JH, Heffner DM (2013) New constraints on buried Triassic basins and regional implications for subsurface CO_2 storage from the SeisData6 seismic profile across the South East Georgia Coastal Plain. Environ Geosci 20(1):1–13

Albritton DL, Meira Filho LG (2001) The scientific basis: contribution of working group I to the third assessment report of the

intergovernmental panel on climate change technical summary. IPCC, Geneva

Bachu S, Gunter WD, Perkins EH (1994) Aquifer disposal of CO_2: hydrodynamic and mineral trapping. Energy Convers Manag 35:269–279

Burruss RC, Brennan ST, Freeman PA, Merrill MD, Ruppert LF, Becker MF, Herkelrath WN, Kharaka YK Neuzil CE, Swanson SM, Cook TA, Klett TR, Nelson PH, Schenk CJ (2009) Development of a probabilistic assessment methodology for evaluation of carbon dioxide storage: USGS, Open File Report 1035, pp 1–44

Chowns TM, Williams CT (1983) Pre-Cretaceous rocks beneath the Georgia Coastal plain—regional implications. In: Gohn GS (ed) Studies related to the Charleston, South Carolina, earthquake of 1886—tectonics and seismicity: US Geological Survey Professional paper 1313, pp L1–L42

Core Laboratories (1984) Analysis report. Texaco Inc. Essex Exploration and Production Company, Norris C. Lightsey No. 1 Well Wildcat, Collenton County, South Carolina

Daniels DL, Zietz I, Popenoe P (1983) Distribution of subsurface lower Mesozoic rocks in the Southeastern United States as interpreted from regional aeromagnetic and gravity maps. In: Gohn GS (ed) Studies related to the Charleston, South Carolina earthquake of 1886-Tectonics and Seismicity. U.S. Geological Survey Professional Paper 1313, pp K1–K24

DOE (2008) Methodology for development of geologic storage estimates for carbon dioxide, DOE Regional Carbon Sequestration Partnerships, pp 27–30

EIA (2007) Short-term energy outlook-June 2007. Energy Information Administration (EIA), Washington

Gohn GS (1983) Geology of the basement rocks near Charleston, South Carolina—data from detrical rock fragments in lower Mesozoic(?) rocks in Clubhouse Crossroads test hole #3. In: Gohn GS (ed) Studies related to the Charleston, South Carolina, earthquake of 1886—tectonics and seismicity: US Geological Survey Professional Paper 1313, pp E1–E22

Gohn GS, Houser BB, Schneider RR (1983) Geology of the lower Mesozoic(?) sedimentary rocks in Clubhouse Crossroads test hole #3 near Charleston, South Carolina. In: Gohn GS (ed) Studies related to Charleston, South Carolina earthquake of 1886—tectonics and seismicity: US Geological Survey Professional Paper 1313, pp D1–D17

Goldberg DS, Kent DV, Olsen PE (2010) Potential on-shore and off-shore reservoirs for CO_2 sequestration in Central Atlantic Magmatic Province Basalts (CAMP). PNAS 107(4):1327–1332

Gottfried D, Annell CS, Byerly GR (1983) Geochemistry and tectonic significance of subsurface basalts near Charleston, South Carolina; Clubhouse Crossroads test holes #2 and #3. In: Gohn GS (ed) Studies related to Charleston, South Carolina earthquake of 1886—tectonics and seismicity: US Geological Survey Professional Paper 1313, pp A1–A19

Grana D, Della Rossa E (2010) Probabilistic petrophysical properties estimation integrating statistical rock physics with seismic inversion. Geophysics 75(3):O21–O37

Hames WE, Renne PR, Ruppel C (2000) New evidence for geologically instantaneous emplacement of earliest Jurassic Central Atlantic magmatic province basalts on the North American margin. Geology 28(9):859–862

Heffner DM, Knapp JH, Akintunde OM, Knapp C (2012) Preserved extent of Jurassic flood basalt in the South Georgia Rift: a new interpretation of the J horizon. Geology 40(2):167–170

Hovorka SD, Smyth RC, Paine J, Tinker S, Duncan I (2006) Downscaling capacity estimates from a regional to a site scale—case study in the South Eastern US Gulf Coast Carbon Center at the Bureau of Economic Geology. University of Texas, Austin

Ketcham RA, Carlson WD (2001) Acquisition, optimization and interpretation of X-ray computed tomographic imagery: applications to the geosciences. Comput Geosci 27:381–400

Koide H, Tazaki Y, Noguchi Y, Nakayama S, Iijima M, Ito K, Shindo Y (1993) Subterranean containment and long-term storage of carbon dioxide in unused aquifers and in depleted natural gas reservoirs. Energy Convers Manag 33(5–8):619–626

Lanphere MA (1983) 40Sr/39Ar Ages of basalt from clubhouse crossroads test hole #2, near Charleston, South Carolina, Earthquake of 1886—tectonics and seismicity. United States Geological Survey Professional Paper 1313, pp B1–B8

Lindholm RC, Hazlett JM, Fagin SW (1979) Petrology of Triassic-Jurassic conglomerates in the Culpeper basin,Virginia. J Sediment Petrol 49(4):1245–1261

Lucier A, Zoback MD, Gupta N, Ramakrishnan TS (2006) Geomechanical aspects of CO_2 sequestration in a deep saline reservoir in the Ohio River Valley region. Environ Geosci 13:1–19

Lumley D, Sherlock D, Daley T, Huang L, Lawton D, Masters R, Verliac M, White D (2010) Highlights of the 2009 SEG summer research workshop on CO_2 sequestration. Lead Edge 29(02):138–145

Marine W (1974) Geohydrology of buried Triassic basin at Savannah River plant, South Carolina. Am Assoc Pet Geol Bull 58(9):1825–1837

Marine W, Siple GE (1974) Buried Triassic basin in the central Savannah River area. Geol Soc Am Bull 85:311–320

Mavko G, Mukerji T, Dvorkin J (2003) The rock physics handbook. Cambridge University Press, UK

McBride JH, Nelson KD, Brown LD (1989) Evidence and implications of an extensive early Mesozoic rift basin and basalt/diabase sequence beneath the southeast Coastal Plain. Geol Soc Am Bull 101:512–520

McGrail BP, Schaef HT, Ho AM, ChienY, Dooley JJ, Davidson CL (2006) Potential for carbon dioxide sequestration in flood basalts. J Geophys Res 111:1–13. Article No B12201

Miall AD (1996) The geology of fluvial deposits. Springer, Berlin

Nelson PH (2004) Permeability-porosity data sets for sandstones. Lead Edge 23:1143–1144

Olsen PE, Froelich AJ, Daniels DL, Smooth JP, Gore JW (1991) Rift basins of early mesozoic age, the geology of the Carolinas, Carolina Geological Society 50th Anniversary Volume, pp 142–170

Petersen TA, Brown LD, Cook FA, Kaufman S, Oliver JE (1984) Structure of the Riddleville basin from COCORP seismic data and implications for reactivation tectonics. J Geol 92:261–271

Planke S, Alvestad E, Eldholm O (1999) Seismic characteristics of basaltic extrusive and intrusive rocks. Lead Edge 18:342–348

Prasad M (2002) Acoustic measurements in unconsolidated sands at low effective pressure and overpressure detection. Geophysics 67(2):405–412

Prasad M (2003) Velocity-permeability relations within hydraulic units. Geophysics 68(1):108–117

Reid MS, Aucott RW, Lee RW, Renken RA (1986) Hydrologic and geologic analysis of a well in Dorchester County, South Carolina: US Geological Survey Water-Resources Investigation Report 86-4161, p 23

Schaef HT, McGrai BP, Owen AT (2009) Basalt-CO_2-H_2O interactions and variability in carbonate mineralization rates, science direct. Energy Procedia 1:4899–4906

Schon JH (2011) Physical properties of rocks. Elsevier, UK

Smyth RC (2007) Potential sinks for geologic storage of carbon dioxide generated in the Carolinas. US Bureau of Econ Geol, Summary Report 1–14

Spikes K, Mukerji T, Dvorkin J, Mavko G (2007) Probabilistic seismic inversion based on rock-physics models. Geophysics 72(5):R87–R97

Tans P (2012) Trends in atmospheric carbon dioxide at Mauna Loa. US Department of Commerce NOAA (National Oceanic and

Atmospheric Administration). http://www.esrl.noaa.gov/gmd/ccgg/trends/. Accessed 27 December 2012

Traverse (1987) Pollen and spores date origin of rift basins from Texas to Nova Scotia as early late Triassic. Science 236:1469–1472

Wyllie MRJ, Gregory AR, Gardner LW (1956) Elastic wave velocities in heterogeneous and porous media. Geophysics 21:41–70

Ziegler PA (1983) Hydrocarbon potential of the Newark rift system: eastern North America. Northeast Geol 5(3/4):200–208